Defense Technical Information Center Compilation Part Notice

ADP012083

TITLE: Control of Supercavitation Flow and Stability of Supercavitating Motion of Bodies

DISTRIBUTION: Approved for public release, distribution unlimited

This paper is part of the following report:

TITLE: Supercavitating Flows [les Ecoulements supercavitants]

To order the complete compilation report, use: ADA400728

The following component part numbers comprise the compilation report:
ADP012072 thru ADP012091

Control of Supercavitation Flow and Stability of Supercavitating Motion of Bodies

Yu. N. Savchenko
Ukrainian National Academy of Sciences - Institute of Hydromechanics
8/4 Zhelyabov str., 03057 Kiev
Ukraine

Introduction

Control of the supercavity parameters is necessary for maintenance of calculated regime of the supercavitation flow in unsteady conditions: at changing the velocity and depth of the body motion. The problem of cavitation flow control includes the two problems connected among themselves:

I) the control of cavity dimensions;

II) the control of forces on a cavitating body.

We consider sequentially both problems.

I) It is known [1, 2] that at small σ the mid-section diameter D_c and length L_c of the axisymmetrical cavity are determined by the cavitator diameter D_n, the drag coefficient c_x and the cavitation number:

$$\frac{D_c}{D_n} = \sqrt{\frac{c_{x0}\ (1+\sigma)}{\sigma}}, \qquad \frac{L_c}{D_n} = \frac{1}{\sigma}\sqrt{c_{x0}(1+\sigma)\ln\frac{1}{\sigma}}. \tag{1}$$

where the cavitation number $\sigma = 2(\rho g h - p_c)/\rho V^2$ is a an important parameter of supercavitating flows. Here, h, V are the depth and the speed of motion, respectively, and p_c is the cavity pressure.

At small cavitation numbers [6] the following approximate formula for the drag coefficient of a blunted cavitator is valid:

$$c_x = c_{x0}(1+\sigma), \tag{2}$$

where c_{x0} is the drag coefficient value for a given cavitator when $\sigma = 0$ (that is, for free streamline flow).

The validity of asymptotic relations (1) for models with disk cavitator moving with velocities $300 \div 1300$ m/s is confirmed by us experimentally [3].

It is visible from relations (1) that at constant D_n, h, V to control cavity dimensions it is possible by two ways:

1) changing the cavitation number σ; 2) changing the cavitator drag coefficient c_x.

Paper presented at the RTO AVT Lecture Series on "Supercavitating Flows", held at the von Kármán Institute (VKI) in Brussels, Belgium, 12-16 February 2001, and published in RTO EN-010.

1. Supercavitation flow control by gas blowing

The first way is effective at motion velocities $10 \div 100$ m/s and is realized by gas supply to the cavity, i.e. by increase p_c (so named the artificial cavitation or ventilation [5]). The method of gas-supply is widely applied in experimental researches for formation of long cavities at moderate flow speeds in the hydrodynamic tunnel (Fig.1).The Fig. 2 demonstrate dependencies $\sigma = \sigma(\overline{Q})$.

The value of gas-supply to the cavity Q is defined by dependence [2, 6]:

$$\overline{Q} = \frac{Q}{VD_n^2} = F(\sigma, Fr, \mathrm{Re}, We), \tag{3}$$

where Fr, Re, We are accordingly *Froude, Reynolds* and *Weber* numbers. The Fig. 3 demonstrate the cavity length – L control by gas flow rate $\overline{Q}$. In the region of strong influence of gravity the formula for supply value has the form [2]:

$$\overline{Q} = \frac{0.27}{\sigma[\sigma^3 Fr^4 - 2]}. \tag{4}$$

In the regimes close to vapor ones the structure of dependence (4) changes:

$$\overline{Q} = kVS\left(\frac{\sigma_\upsilon}{\sigma} - 1\right). \tag{5}$$

The region of effective control of air-supply in the artificial cavitation regime is limited by value $\sigma_{\min} = 1.41 g D_c / V^2$ from (4) and by vapor cavitation occurrence at $\sigma = \sigma_v$:

$$1.41 g D_c / V^2 < \sigma \le \sigma_\upsilon = \frac{2(p - p_\upsilon)}{\rho V^2}, \tag{6}$$

where p_υ is the pressure of saturated water vapor.

The motion in water with velocities $V >> 100$ m/s occurs in the regime of vapor or natural cavitation, then the gas-supply to the cavity becomes inefficient.

2. Supercavitation flow control by jet cavitator

According to the hydrodynamic scheme of supercavitation flow, the object is placed partially or fully inside a supercavity (Fig. 4a, b) formed by the nasal part (cavitator) [1, 4, 6]. In the case of a jet cavitator system, the cavity separates from the craft hull (Fig. 4c).

The comparatively new scheme (c) has in comparison with conventional schemes (a) and (b) the following advantages:

1) the hydrodynamic drag reduction due to the model in general has not points of contact with water (theoretically in twice in comparison with a solid disk cavitator at $\sigma \to 0$);

2) the possibility of control of cavity by water rate change in the nose jet.

For the first time *L.I.Sedov* offered the way of formation of cavities due to giving up the fluid jet toward to the mainstream (i.e. scheme of jet cavitator) [4]. He gave the estimation of drag coefficient of the jet cavitator, considering it as an inverted scheme of cavity with reentrant jet [14].

The scheme of cavitating flow around the body A with reentrant jet is presented in Fig. 5a. It is known as the *Efros - Hilbarg* scheme [14]. It is theoretically possible to think that the reentrant jet is absorbed by fictitious body B. Then the cavitation drag of body A is equal to:

$$X = \rho Q(V_\infty + V_c), \quad V_c = V_\infty \sqrt{1+\sigma}, \tag{7}$$

where $Q = SV_c$ is the volumetric water rate in the reentrant jet, S is the area of jet section, V_c is the velocity on the cavity surface (it is equal to velocity in the reentrant jet).

Passing on to the limit at $\sigma \to 0$ (thus the body B tends to the infinity), we obtain the cavitating drag of body A by *Kirchhoff* scheme :

$$X_0 = 2\rho Q V_\infty . \tag{8}$$

Changing the direction of all the velocities at $\sigma \to 0$, we obtain the scheme of cavitating flow around the body B with jet cavitator (Fig. 5b). The expenditure of energy expending by body on overcoming of cavitator drag is replaced by expenditure of energy on formation of opposing jet in this case. We obtain for jet momentum:

$$\rho Q V_\infty = \frac{X_0}{2}, \tag{9}$$

i.e. when $\sigma \to 0$, the opposing jet momentum necessary for cavity supporting is twice less than cavitating drag force of a solid cavitator.

We experimentally investigated the cavities formed by opposing liquid jet in the small hydrodynamic tunnel at the IHM UNAS at flow velocity 10 m/s. Thus the air is in addition supplied to the cavity because of small flow velocity. The experimental dependence of opposing jet length L_j from the nozzle to the frontal point of cavity on velocity in the jet $\overline{V}_j = V_j / V_\infty$ is presented in Fig. 6.

We note that the limit value obtained experimentally $V_j(L_j) \approx 0.75 V_\infty$ at $L_j \to 0$ does not correspond to the classical scheme of jet collision with critical point [14], in which $\rho V_\infty^2 = \rho V_j^2$. The value $V_j(0) \approx 0.75 V_\infty$ permits to assume that the scheme of jet collision with formation of critical region without breakdown points [14] is realized in the experiment. For such scheme the relation $\rho V_\infty^2 = 2\rho V_j^2$ should be fulfilled theoretically, whence $V_j = 0.707 V_\infty$.

We mention yet for completeness about a cavitating flow scheme similar externally to the scheme where the cavity is formed with help of gas jet blown out from the model nose toward mainstream [5]. Thus these cavities relate to artificial (ventilated) cavities by classifications. To create cavity the gas jet with density ρ_g should be blown out with velocity V_g enabling to overcome the dynamic head of water mainstream $\rho V_\infty^2/2$. We have from the *Bernoulli* integral:

$$V_g > V_\infty \sqrt{\frac{\rho}{\rho_g}(1+\sigma)}. \tag{10}$$

If the air is used as a gas $\rho/\rho_g = 800$, then we obtain from (10) without account of air compressibility:

$$V_g > 28.3\left(1+\frac{\sigma}{2}\right)V_\infty.$$

It is visible that such way of cavity formation is really realized only at small V_∞.

The conducted experiments show that the cavities created due to opposing gas jet have the strongly disturbed surface and the powerful accompanying turbulent emulsion flow [5].

3. Supercavitation flow control by change of c_x

As it is was said above the cavity control method by means of gas-supply is not applied at very high velocities of motion in water and/or small model dimensions. Therefore, the research of possibility of cavity control by change of c_x is very interesting.

3.1. ESTIMATION OF DRAG OF AXISYMMETRIC CAVITATOR

The practical way of estimation of the drag of the axisymmetric cavitators consists in that the pressure distribution p along the generator of cavitator is taken from the solution of the two-dimensional problem on free streamline flow around the contour coinciding with a meridian section of the cavitator. Then the drag of the axisymmetric cavitator is defined by integration:

$$\tilde{c}_x = \frac{2\tilde{X}}{\rho V^2 \pi R_n^2}, \quad \tilde{X} = 2\pi \int_0^{R_n} (p - p_c) y dy, \tag{11}$$

where $R_n = D_n/2$.

It was shown in the work [17] that the values c_x for cones computed by given approximate way are close to the experimental data. We present also their comparisons with results of the numerical computation executed on basis of exact formulation of the problem [18]. For comparison we use the approximation formulae given in the work [19]:

$$
\begin{aligned}
c_x &= c_{x0} + (0.524 + 0.672\mu)\sigma, 0 \le \sigma \le 0.25, \\
&\qquad \frac{1}{12} \le \mu \le \frac{1}{2}, \\
c_{x0} &= 0.5 + 1.81(\mu - 0.25) - 2(\mu - 0.25)^2, \\
&\qquad \frac{1}{12} \le \mu \le \frac{1}{2} \\
c_{x0} &= \mu(0.915 + 9.5\mu), \ 0 < \mu < \frac{1}{2},
\end{aligned}
\tag{12}
$$

where $\mu\pi$ is the half angle of cone. When $\sigma \to 0$, the values c_{x0} are obtained by extrapolation method. A comparison of the experimental data with the results of "exact" [19] and approximate [17] computations is given in Table 1:

Table 1

$\pi\mu$ (deg.)	15	30	45	60	75	90
Exper.	0.15	0.35	0.47	0.61	0.72	0.82
c_{x0} [7]	0.1428	0.3353	0.5000	0.6369	0.7461	0.8275
$\widetilde{c}_{x0}$ [10]	0.2045	0.3758	0.5181	0.6350	0.7296	0.8053

We obtain the calculated formula for an arbitrary contour from (11):

$$
\widetilde{c}_{x0} = \frac{2}{R_n^2} \int_0^1 \overline{p}(\eta) y(\eta) \frac{dy}{d\eta} d\eta . \tag{13}
$$

3.2. CAVITATOR WITH VARIABLE DRAG

Both the length and the biggest diameter of cavity are proportional to $\sqrt{c_{x0}}$ as it is seen from the relations (1).

$$\frac{D_c}{D_n} = \sqrt{\frac{c_{x0}\ (1+\sigma)}{\sigma}}, \qquad \frac{L_c}{D_n} = \frac{1}{\sigma}\sqrt{c_{x0}(1+\sigma)\ln\frac{1}{\sigma}}. \tag{14}$$

Hence, the cavity shape should change similarly to self at changing the control parameter c_{x0} when D_n and σ are constant. It may be obtained by changing the cavitator shape at constant diameter of the cavitating edge.

We offer the sketch of the axisymmetric cavitator with variable geometry. The meridian section of the cavitator has the $\sum$ – shaped contour. The cavity drag coefficient is increased from $c_x(\beta)$ up to 1 for a cone at moving of the internal cone relatively to the outside cartridge with a cavitating edge, i.e. at increase of parameter x/D_n from 0.

The graphic of dependence c_{x0} on x/D_n is shown in Fig. 7 for $\sum$ – shaped contours.

The graphic of dependence of the ratio $\widetilde{c}_{x0}$ for axisymmetrical cavitators to theoretical value of the drag coefficient for disk 0.8053 on the dimensionless extension of cavitating edge x/D_n is shown in Fig. 8. Also, the experimental points are plotted there. As it is seen, the drag increases slower in the experiment than as the computation predicts at increase of x. It is explained that the closed zones of vortical motion of water are formed in the interior angles of cavitator in the experiment. Other words, the potential scheme of the free streamline flow with the critical point is not realized in this case, but the scheme of the flow with stagnant zones is realized [14].

The appearance of cavity at the two extreme positions of cone $(\sigma = 0.077, \mu = 1/3)$ is given in Fig. 9. At extending of cavitating edge from $x/D_n = 0$ to $x/D_n = 0.138$ in the experiment we obtained the increase of main dimensions of cavity on 35 %.

4. Stability of supercavitating motion of bodies

4.1. POSSIBLE FLOW SCHEMES

The analysis showed that the four different mechanisms of motion stabilization sequentially act at motion velocity increase.

1. Two-cavity flow scheme (Fig. 10a), $V \sim 70$ m/s.

In this case the hydrodynamic drag center is placed behind the mass center, and stabilizing moment of the force Y_2 acts to the model. It means that the classic condition of stability is fulfilled.

2. Stationary planing along the internal surface of cavity (Fig. 10b), $V \sim 50 \div 200$ m/s. To compensate the buoyancy losses the body's tail part is planing along the lower internal cavity surface. In this case the motion may be stable as a whole.

3. Impact interaction with cavity boundaries (Fig. 10c), $V \sim 300 \div 900$ m/s. Presence of initial perturbations of the model attack angle and the angular velocity causes to the impact of the model tail part against the internal boundary of cavity. The mathematical modeling showed that after this impact the model can perform steady or damped oscillations accompanied by periodic impacts of the tail part alternately against the upper and lower cavity walls. Then the motion can remain stable as a whole.

4. Aerodynamic interaction with vapour-splash medium of cavity (Fig. 10d), $V \sim 1000$ m/s **and higher**. At very high velocities the aerodynamic and splash forces of interaction with vapour filling the cavity and splashes near the cavity boundaries have considerable effect on the body motion. Since the clearance between the body surface and the cavity boundary usually is small compared to the cavity radius, we apply the known methods of near-wall aerodynamics to estimate the arising forces.

Statically stable contours

The pressure forces acting on the inclined contours in free streamline flow sum to the resultant force $\vec{F}$

and moment M_0 shown in Fig. 11.

The contour will be statically stable if these forces tend to turn the cavitator to decrease angle α relative to the mass center of the model. The condition of static stability has the form:

$$\delta = \arctan\frac{F_y}{F_x} > \alpha, \tag{15}$$

where F_x and F_y are the projections of the vector $\vec{F}$ onto the x- y-axes.

Computations have shown that a cavitator is statically stable if its contour is concave towards to the stream (in particular, inverted wedges with $\mu > 0.5$). A flat plate will be neutrally stable, $F_y / F_x = \tan\alpha$, if we do not take into account the moment M_0 induced by displacement of point of application of force $\vec{F}$ from the point C. Computations have shown that this moment is always stabilizing, but is very small in value. Convex contours (in particular, wedges with at $\mu < 0.5$) are statically unstable.

The force polars for wedges are shown in Fig. 12 for a series of values of wedge semiangle $\beta = \pi\mu$ in degrees. The characteristic stability regions are shown in Fig. 13. Wedges are statically stable for $\beta > 90^\circ$, and are statically unstable for $\beta < 90^\circ$. The lift of a wedge is equal to 0 irrespective of the attack angle for $\beta \approx 50^\circ 35'$ [9].

Computer program FLOWJET allows to select the best cavitator shape for static stability when the arbitrary c_y^α is maximum. The best cavitator from a practical point of view: (1) is statically stable; (2) has a maximal rotational derivative c_y^α; and (3) has a minimal drag coefficient c_{x0}.

4.2. DESIGNING THE SUPERCAVITATING (SC) MODELS

The supercavitation flow scheme is a special artificial scheme. It is necessary to know a cavity shape for successful realization of this scheme. This is necessary for optimal location of the body in the supercavity.

We consider two problems:

– calculation of a supercavity for a body of given shape and given motion regime;

– design of optimal body shape for the known supercavity.

Stage I. Inscribing the body into the cavity

According to the given motion regime – $V = V(t)$; $H = H(t)$ we calculate minimal and maximal cavitation numbers

$$\sigma_{\min} = \sigma(V_{\max}; H_{\min}); \quad \sigma_{\max} = \sigma(V_{\min}; H_{\max})$$

to construct minimal and maximal supercavity contours $R = F(Rn; \sigma)$ past a circular disk [16].

The main purpose of this stage is to inscribe the model into the minimal cavity contour. The minimal contour is determined by presence of points of contact of the model contour and the free cavity boundary in the tail part.

Fig. 14 presents results of the computation of cavity shape past disk cavitators around the body of revolution. These results are obtained with the help of software SCAV developed at IHM UNAS. The program permits to plot supercavities by given parameters: diameter and angle of the cavitator D_n; β; velocity V and depth H of the motion; the pressure in the cavity P_c.

At that we determine the clearance h between the body surface and the cavity boundary, ring area of this clearance along the whole body length, moment of inertia and body mass (Fig. 15).

The program also computes the distance and the velocity reduction from the starting velocity $V = V_0$ upon motion on inertia and displays graphs of changing the length L_c and diameter D_c of the supercavity as well.

Stage II. Optimization of the supercavitating body contour

This stage purpose is to optimize the clearance between the free cavity boundary and model.

During motion of the model by given regime ($V = V(t)$, $H = H(t)$) the supercavity shape will change according to changing the cavitation number

$$\sigma_{\min} \le \sigma \le \sigma_{\max}.$$

The clearance between the body and cavity boundary will be changed in certain range according to changing of σ.

Besides the clearance will be changed under action of possible angular oscillations of the model about the center of mass in supercavities with dimensions exceeding the minimal possible ones $(\sigma > \sigma_{\min})$.

Fig. 16 shows a PC-screen copy of optimization procedure for the model shape at its angular inclination ψ. Simultaneously, values of upper h_2 and lower h_1 clearances between the model and supercavity contours are shown there. The program STAB permits to determine the maximal angles of trim $\psi = \psi_{\max}$, points of touching the model with the cavity and the mass center location. A simple rule was developed for ensuring the stability of the supercavitating model motion at the IHM UNAS.

Rule of optimization of SC model shape

For certain ranges of varying the cavitation number $\sigma_{\min} \le \sigma \le \sigma_{\max}$ and angles of trim $\psi \le |\psi_{\max}|$, the optimal shape of the supercavitating model must not have points of touching with the supercavity contour which are situated in front of the model center of mass.

This requirement does not take into account the dynamics of the body and is based on principles of static stability. In the case of continuous flow the analogous rule of the stable motion maintenance requires location of a point of the hydrodynamic force application past the body center of mass. Both the rules guarantee against appearance of destabilizing moments directed to the possible angle of model deflection. This means that the induced total moment acting on the model always must has a sign opposite to a sign of angle ψ – accidental deflection of the model

$$Sgn\, M = -Sgn\, \psi\ .$$

4.3. EQUATIONS OF THE SCM DYNAMICS

The most effective method of investigation of the supercavitating body dynamics proved to be its direct simulation on a PC-screen (computer experiment). It permits to research the motion stability in interactive regime "researcher – computer" [16].

The complete mathematical model of the SCM motion includes a set of equations of solid body dynamics, equations to calculate the unsteady cavity shape and relations to calculate the acting forces.

A set of dynamic equations of the axisymmetric body motion in vertical plane without rotation in the body co-ordinate system $O_1 x_1 y_1$ is

$$m\left(\frac{d\vec{V}}{dt} + \vec{\omega} \times \vec{V}\right) = \Sigma \vec{F}\ , \tag{16}$$

$$I_c \frac{d\vec{\omega}}{dt} = \Sigma \vec{M}_z \tag{17}$$

where $\vec{V} = \{V_x, V_y, 0\}$ is the velocity of the SCM mass centre; $\vec{\omega} = \{0, 0, \omega\}$ is the angular velocity; m is the mass of model; I_c is the moment of inertia of model about mass centre.

Passing on to the integration along the longitudinal absolute co-ordinate x and adding obvious kinematic relations, we obtain the calculation set of five ordinary differential equations

$$V\cos(\psi-\alpha)\frac{dV_x}{dx}=\omega V_y+\frac{1}{m}\Sigma F_x, \tag{18}$$

$$V\cos(\psi-\alpha)\frac{dV_y}{dx}=-\omega V_x+\frac{1}{m}\Sigma F_y, \tag{19}$$

$$V\cos(\psi-\alpha)\frac{d\omega}{dx}=\frac{1}{I_c}\Sigma M_z, \tag{20}$$

$$V\cos(\psi-\alpha)\frac{d\psi}{dx}=\omega, \tag{21}$$

$$\frac{dy}{dx}=\tan(\psi-\alpha). \tag{22}$$

Here, ψ is the model pitch; α is the angle of attack; y is the ordinate of the SCM mass centre in the absolute co-ordinate system (see Fig. 17).

4.4. RELATIONS FOR FORCES AND MOMENTS

Two kinds of forces in right parts of Eqs. (18) – (20) are essential in considered velocity range (see Fig. 17):

– hydrodynamic force and moment on the cavitator $\vec{F}_n$, $\vec{M}_n$;

–hydrodynamic force and moment due to interaction between the SCM tail and internal cavity wall $\vec{F}_x$, $\vec{M}_x$.

Coefficients of the force projections acting on the cavitator-disk inclined to the stream at angle α are approximately calculated by formulae [2]:

$$c_x=c_{x0}\cos^2\alpha,\quad c_y=c_{x0}\sin\alpha\ \cos^2\alpha. \tag{23}$$

For disk cavitators with plane perpendicular to the model axis, the vector $\vec{F}_n$ is always directed along the model axis. Therefore, the force on the cavitator does not create any moment. Formulae (23) agree with experiment for a disk and blunted cavitators when $\alpha<50^\circ$.

We use the approximate method [9] to calculate the hydrodynamic force on inclined non-disk cavitator. It is based on the exact solution of the two-dimensional problem on free jet flow around an inclined polygonal contour.

Process of interaction between the SCM tail and internal cavity wall is considered as unsteady planing of a prolate body along the curvilinear liquid boundary. The forces arising in this case are calculated basing on the hypothesis of plane sections [2]. The solution of the problem on immersion of the circular arc through the curvilinear boundary is used in this case [20].

If both the middle clearance $\Delta = R_c - R_s$ and the model immersion depth into the cavity surface h_k are small, formula for the cross component of the tail force in the body coordinate system was obtained in the form [20]

$$F_{sy} = \rho \pi R_s^2 V \left[V_1 \frac{\overline{h}\left(2+\overline{h}\right)}{\left(1+\overline{h}\right)^2} + V_2 \frac{2\overline{h}}{1+\overline{h}} \right], \tag{24}$$

where R_s is the stern section (transom) radius of the model; V_1 is the cross velocity of the model transom; $V_2 = -\partial R_c / \partial t$ is the velocity of the cavity boundary; $\overline{h} = -h_k / \Delta,\ k = 1.2;\ h_1 < 0,\ h_2 < 0$ is the model transom immersion into the lower and upper cavity boundaries, respectively.

The longitudinal component of force F_{sx} has viscous nature and is calculated by formulae

$$F_{sx} = \frac{\rho V^2}{2} S_w c_f \left(\mathrm{Re}\right), \tag{25}$$

where S_w is the area of washed part of the model; c_f is the viscous drag coefficient; Re is the *Reynolds* number.

If the motion velocity is very high $V > 1000$ m/s, then aerodynamic forces of interaction between the model body and vapour-gas-spray medium filling the cavity can essentially influence on the SCM dynamics [1]. Our evaluations have shown that this influence has damping character [20].

4.5. STABILITY OF SCM MOTION

Computer simulation with the STAB software allows to investigate the stability of SCM motion "as a whole", when the model oscillates within the cavity ricocheting by its tail from lower and upper cavity walls in turn.

The PC-screen view after execution of the function “Motion” is shown in Fig. 18, a. Here, *HX* is the dimensionless calculation step; $N = 10$ is the number of the model contacts with upper and lower cavity contours. The velocities V_x, V_y and ω are output in dimensionless by L, V_0 form (where L is length of the model). The angles ψ, α are output in radians. A signs of the coefficients show the direction of the force and moment action.

The PC-screen view after execution of the function “History” for the same model and starting data is shown in Fig. 18, b. The *y*-coordinates of the graphs are plotted in dimensionless form, the *x*-coordinate *x* is given in meters. As it is visible from graphs, the interaction of the SCM tail and water has behaviour of short-term impulses. It is displayed in discontinuous behaviour of functions $\omega(x)$ and $V_y(x)$ [16].

The performed analysis has shown that the motion stability of the SCM with a disk cavitator is determined by three dimensionless parameters:

$$\bar{I}_c = \frac{I_c}{mL^2}, \quad St = \frac{\omega_0 L}{V_0}, \quad \overline{\Delta} = \frac{R_c - R_s}{R_n}.$$

Value of the parameter $\overline{\Delta}$ is determined mainly by cavitator radius R_n for given model shape and weakly depends on starting velocity V_0.

After a number of calculations at constant values of $V_0, \bar{I}_c, x_2$ and varied values of R_n, ω_0, the plane of the parameters $\overline{\Delta}, St$ is divided on the zone I where motion is stable and the zone II where the motion is unstable. For dynamically similar models $\bar{I}_c = const$ the stability zones are equal.

The motion stability loss is visually perceived on the PC-screen as washing the frontal part of model and inadmissible great increase of the pitch ψ.

Also, the STAB software permits to simulate the regime of continuous planing the model along the lower cavity wall including the ventilated one and with working propulsor. In this case, the cavitator is fixed at the angle of δ to the model axis to compensate the moment of the force arising on the tail. Thrust of the propulsor is added to the right part of Eq. (18).

The computer simulation that the SCM motion in regime of continuous planing is unstable when the angle δ is constant.

4.6. COMPARISON WITH EXPERIMENT

We confirmed reality of the SCM self-stabilisation mechanism by ricocheting from the cavity walls by direct shooting the motion in water with velocities up to 1200 m/s [4, 6]. In experiment, its action appears in periodic supercavity surface perturbations which develop next according to the "independence principle". In Fig. 19, the experimental photographs of the model in moment of touch to the cavity wall (compare with Fig. 14, a) and the supercavity part perturbed after contact with model are shown. In this case, the exposure time of shooting was $3 \cdot 10^{-6}$.

Asymmetric washing the model occurs when the SCM motion loses stability. It results in impact increase of the hydrodynamic drag and deformation of model.

5. Schemes of the hydrodynamic stabilization and control of SC objects

5.1. SCHEME WITH FREE PLANING ALONG A CAVITY

This scheme (Fig. 20) of the vehicle motion is more favorable, because has the smallest washed part of the body and, hence, the lowest hydrodynamic drag. However, this scheme of motion will have essential distinctions in creation of stabilizing hydrodynamic forces.

At motion the vehicle is located in the cavity under some angle of attack α_A. It stipulates the appearance of lift on the tail part due to asymmetric washing the cylindrical part of the body. At motion with constant velocity V_∞ and depth H (or the pressure $P_0 = \rho g H$) we can choose the constructive parameters of the vehicle:

– position of gravity center;

– cavitator dimensions;

– deflection angle of α_P;

– gas-supply value of the artificial cavity Q or its length $L_C = F(Q)$ so that the basic conditions of the motion stability (equality of projection of all forces and moments acting on the body in the uniform rectilinear motion) are fulfilled:

$$\begin{aligned} Y_C + Y_B &= G - T\sin\alpha_A, \\ X_C + X_B &= T\cos\alpha_A, \\ M_C + M_B &= 0. \end{aligned} \tag{26}$$

The hydrodynamic forces on the cavitator at deflection on small angle α_C can be determined by formulae [13]

$$\begin{aligned} Y_C &= X_{C0}\cos\alpha_C \sin\alpha_C, \\ X_C &= X_{C0}\cos^2\alpha_C, \end{aligned} \tag{27}$$

where X_{C0} is the cavitator drag at $\alpha_C = 0$. For a disk:

$$X_{C0} = 0.82\frac{\rho V^2}{2}S_0,$$

where S_0 is the area of the cavitator section on the cavitating edge; $\alpha_C = \alpha_P - \alpha_A$ is the cavitator angle of attack; α_P is the positional angle of the cavitator fixation; α_A is the body's angle of attack; X_B is the drag of washed part of the body which includes the friction drag of the side surface X_F.

At this flow scheme it is possible to save the traditional principle of stabilization and control due to the tail fins and rudders, but with an additional condition - the cross stability preservation.

Really, at presence of roll angle, γ, the lift on the cavitator deflected on angle α_C will form the side force $Z_C = Y_C \sin\gamma$, which causes to the body yaw (Fig. 21).

The cross stabilization of the object can be obtained by following ways:

a) due to the location of mass center lower than a line connecting the points Y_C, Y_B of application of the forces (Fig. 22). The stabilizing moment M_γ arises at arising the roll γ, (Fig. 22). In this case it is possible to stabilize the object without fins at all at sufficient magnitude of M_γ

$$M_\gamma = G h_c \sin\gamma; \tag{28}$$

b) due to the hydrodynamic fins of roll (Fig. 23) creating the stabilizing moment.

A possible scheme of cross stabilization of the body within the cavity due to two fins is shown in Fig. 23.

There the tail part of the vehicle is equipped by two supercavitating fins creating hydrodynamic lifts: the right, Y_1 and left, Y_2. At possible angle of roll of the vehicle on angle \gamma the stabilizing moment M_γ must arise due to a difference of these forces caused by various immersion of the right and left fins into flow through the free cavity boundary. The total lift of the two fins must not exceed $10 \div 15$ of the total lift, Y_B, on the vehicle tail

$$Y_1 + Y_2 = 0.15 Y_B .$$

The hydrodynamic forces on fins in stable position arise under action of the hull slope about the cavity axis at gravity influence and also flow bend in the back cavity part caused by cavity floating-up effect.

Stabilization in horizontal plane is achieved due to using a number of factors:

– stabilizing influence of the hydrodynamic forces of washed part of the hull located past the mass center of supercavitating object (SCO);

– application of neutral stability cavitators (disk) relatively to angles of deviation in the horizontal plane;

– using the schemes of a self-stabilization by roll:

– low location of the mass center,

– V-shaped system of fins.

Stabilization of SCO in vertical plane is reached due to the following factors:

– the cavitator with deviation angle having stability about angular deviations in vertical plane (disk, cone $\beta > 110^\circ$) [14];

– stabilizing influence of the washed hull part located past the SCO mass center;

– stabilizing influence of the V-shaped system consisting of two fins located on the tail end of washed part of SCO.

The vehicle completely placed in the cavity is shown in the scheme in Fig. 20. The supporting hydrodynamic forces are created by deflecting statically stable cavitator [14], Y_C, and planing tail part of the vehicle, Y_B.

The low location of a point of the hydrodynamic force, Y_B, application hampers the execution of cross self-stabilization scheme by lowing the mass center *mc* below than a line connecting the points of the hydrodynamic force application on the cavitator, O_C, and on the tail, O_B, of the body (it is shown by dotted line in the scheme).

The considered stabilization schemes do not exclude the application of means of the active control of vehicle for it stabilization during motion.

For SCO control may be used general aerohydrodynamics principle – to realize the object control by using elements creating hydrodynamic side forces as wings, flaps, rudders, jets.

In SC flow scheme the cavitator is a convenient element for side force creation owing formulae (27).

SCO control in horizontal plane

- by cavitator deflection in horizontal plane;
- by cavitator rotation in corresponding side according scheme (Fig. 21);
- by SCO hull rotation in corresponding side by using active fins (Fig. 23).

SCO control in vertical plane

- by cavitator deflection in vertical plane according scheme in Fig. 20 and formula (27).

5.2. OPTIMIZATION OF FIN NUMBER

Traditional stabilization schemes of bodies of revolution with large aspect ratio require presence of two pairs of fins:
– the first pair to stabilize motion in horizontal plane;

– the second pair to stabilize motion in vertical plane [4].

Aerodynamic schemes for stabilization and control were developed to minimize the drag of aircraft and rockets. They have three elements located by 120° or T -shaped and also two elements at V -shaped location [4].

The most of the hydrodynamic high-speed vehicles of known designs have two pairs of fins and rudders for the motion stabilization reliability, control convenience [6] including supercavitating ones [9].

5.3. OPTIMIZATION OF FIN SHAPE

Use of the rudders and fins on supercavitating objects has essential features:
1) two-phase regime of flow around the part or whole fin installed past the artificial supercavity;

2) incomplete washing the fin at possible air layer on the supercavitating object hull in the fin mounting place;

3) high overloads at water entry and take off of the fins at oscillations of the cavity boundary or the body in the supercavity.

Presence of the two-phase flow promotes the flow separation from the frontal edge of the fin and cavity formation. It results in abrupt reduction of the fin lift.

The air layer presence on the hull in the fin mounting place also causes to the lift loss not only due to the loss of the fin interference with the hull. In the case of the plane wall this loss is equal to reduction of the effective aspect ratio λ in two times according to formula for C_y^α:

$$C_y^\alpha = \frac{2\pi}{1+\frac{2}{\lambda}}. \qquad (29)$$

High overloads at abrupt change of medium: water-gas-water require increased strength and increasing the fin profile thickness.

All these features of flow around the rudders and fins on the supercavitating body of revolution were investigated theoretically and experimentally at the IHM UNAS. These research results were development of two-phase profile stable for variable loads [12, 13] and recommendations for the fin shape [14].

All the rudders has wedge profile of the cross section $(\beta = 3^\circ \div 6^\circ)$ (Figs. 24, 25).

The experimental results show that the wedge profile gives more stable flow characteristics for regimes of presence of gas and water-air layers on the body hull. In this case the fins of small aspect ratio $\lambda \leq 1$ are more preferable, because they have no separations in great range of angles of attack.

References

1. Garabedian P.R. Calculation of axially symmetric cavities and jets // Pac. J. Math, 1956. Vol. 6, N 4. P. 611 – 684.
2. Logvinovich G.V. Hydrodynamics of Flow with Free Boundaries.// Kiev, Naukova Dumka, 1969. 208 p. (in Russian)
3. Savchenko Yu.N., Semenenko V.N., Serebryakov V.V. Experimental Study of the Supercavitation Flows at Subsonic Flow Velocities // Doklady AN Ukrainy, 1992, N 2. pp 64 – 69 (in Russian).
4. Sedov L.I. About Ideal Fluid Flow around Body with Counter Jet // Doklady AN SSSR. Vol. 2066. N1. 1972. (in Russian)
5. Yegorov I.T., Sadovnikov Yu.M., Isayev I.I., Basin M.A. Artificial Cavitation. L.: Sudostroenie, 1971. 284 p. (in Russian)
6. Epshtein L.A. Methods of Theory of Dimensionality and Similarity in Problems of Ship Hydromechanics. L.: Sudostroenie. 1970. 207 p. (in Russian)
7. Deynekin Yu.P. Cavitating Flow around Body with Channel. //Hydromehanika. 1994. N. 68. P. 74 - 78 (in Russian).
8. Romanovsky V.I. Symmetric Jet Flow around Contour with Water-Channel //Trudy TZAGY. 1980. N. 2060. P. 31 – 53 (in Russian).
9. Savchenko Yu.N., Semenenko V.N., Naumova Ye.I. Hydrodynamic characteristic of polygonal contours at supercavitating flow// Reports of NAS of Ukraine. 1997. N 7. 97 – 103 (in Russian)
10. Savchenko Yu.N. On motion in water in supercavitation flow regimes//Hydromechanics. 1996. N 70. P. 105 –115 (in Russian)
11. Savchenko Yu.N., Semenenko V.N., Osipenko S.B. Mechanism of Cavity Interaction with Bubble Flow // Doklady AN Ukraini. 1985. N 9. P. 39 – 42 (in Russian).
12. Savchenko Yu.N. Investigation of high-speed supercavitating underwater motion of bodies // High Speed Body Motion in Water (AGARD Report 827). Proc. Fluid Dynamics Panel Workshop. – Kiev, 1997.
13. Vlasenko Yu.D. Experimental investigations of high-speed unsteady supercavitating flows. Proc. Third International Symp. on Cavitation. – Vol. 2. Grenoble (France). 1998. P. 39 – 44
14. Gurevich M.I. Theory of Ideal Fluid Jets (the second edition) N.: Nauka, 1979. 536 p. (in Russian).
15. Savchenko Yu.N., Vlasenko Yu.D., Semenenko V.N. Experimental study of high-speed cavitation flows// Hydromechanics. 1998. N 72. P. 103 – 111 (in Russian)

16. Semenenko V.N. Computer simulation of supercavitating body dynamics// Applied Hydromechanics. 2000. V 2, N 1. P. 57 – 62 (in Russian)

17. Plesset M.S., Shaffer P.A. Cavity drag in two and three dimensions// J. Appl. Phis., 1948. Vol.19, N 10.

18. Guzevsky L.G. Numerical Analysis of Cavitating Flow. Novosibirsk : 1979. (Preprint of Institute of Thermal physics SD of AS Of USSR; N 40 - 79. 36 p. (in Russian).

19. Guzevsky L.G. Approximation Dependencies for Axisymmetric Cavities behind the Cones // Hydrodynamic flows and Wave Processes. Novosibirsk, Institute of Thermophysics of SD of AS of USSR, 1983. P. 82 – 91 (in Russian).

20. Savchenko Yu.N., Semenenko V.N., Putilin S.I. Unsteady processes during supercavitating body motion// Applied Hydromechanics. 1999. V 1, N 1. P. 62 – 80 (in Russian).

21. Knapp R., Daily J., Hammet F. Cavitation. // Mir, Moscow, 1974, 687 p. (in Russian) .

22. Putilin S.I. Some features dynamics of supercavitating models. // J. of Applied hydromechanics, Vol. 2, No 3, 2000, pp. 65 –74.

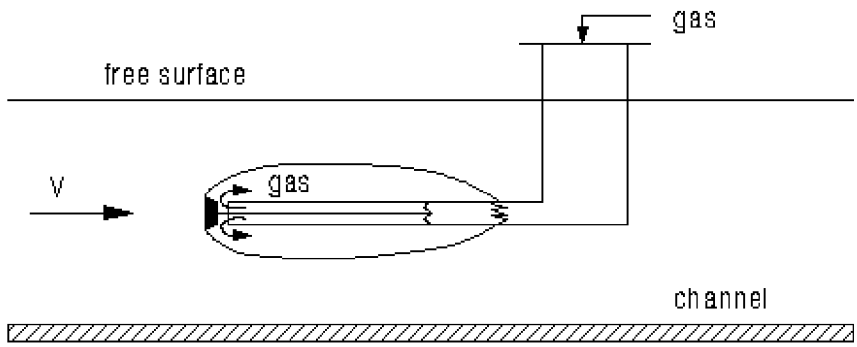

Fig. 1

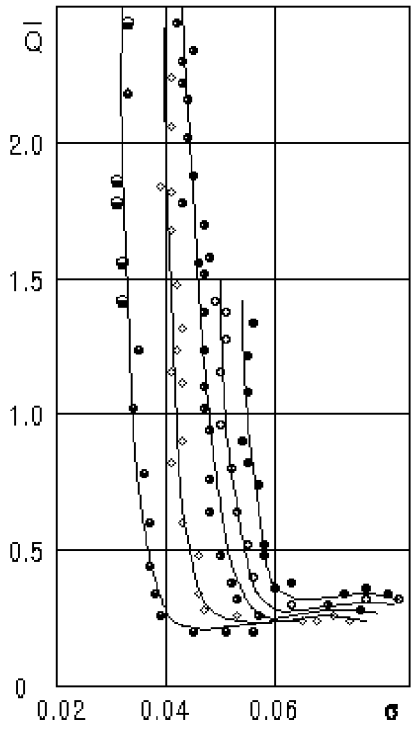

Fig. 2

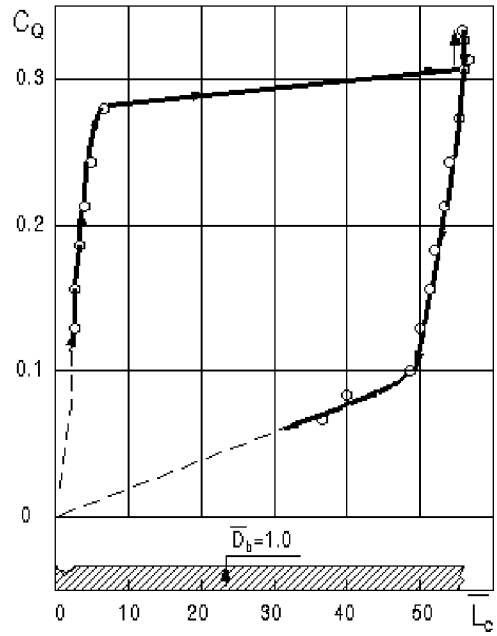

Fig. 3

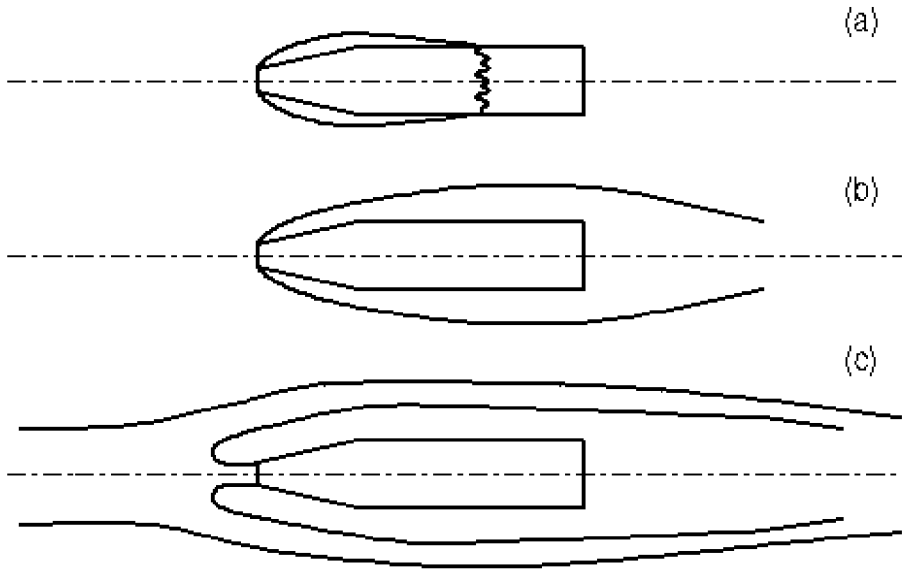

Fig. 4

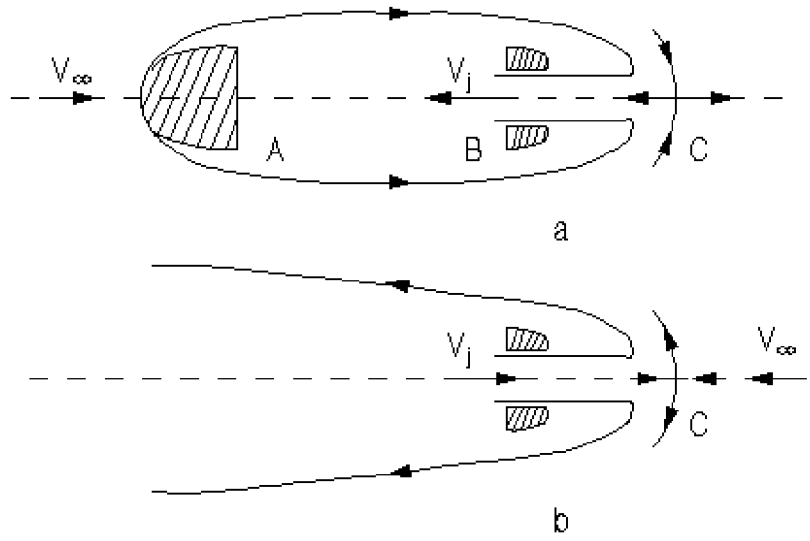

Fig. 5

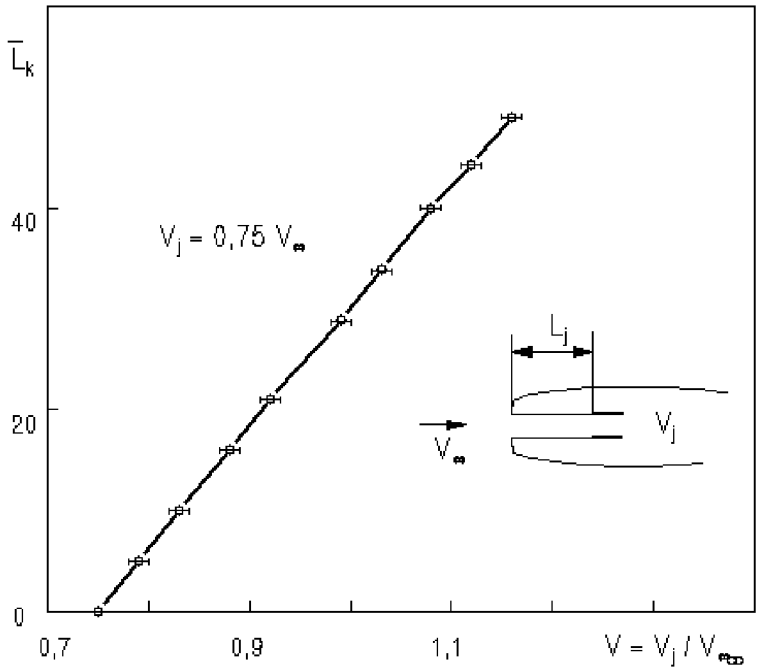
$\bar{L}_k$
40
20
0
V_j = 0,75 V_∞
L_j
V_j
V_∞
0,7
0,9
1,1
$V = V_j / V_\infty$

Fig. 6

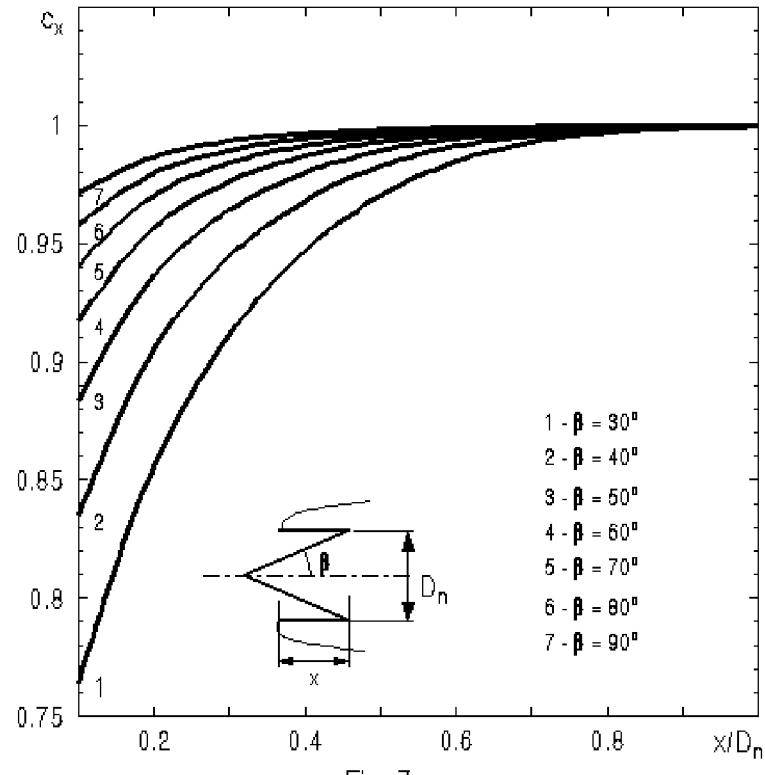
c_x
1
0.95
0.9
0.85
0.8
0.75
0.2
0.4
0.6
0.8
x/D_n
1
2
3
4
5
6
7
1 - β = 30°
2 - β = 40°
3 - β = 50°
4 - β = 60°
5 - β = 70°
6 - β = 80°
7 - β = 90°
β
D_n
x

Fig. 7

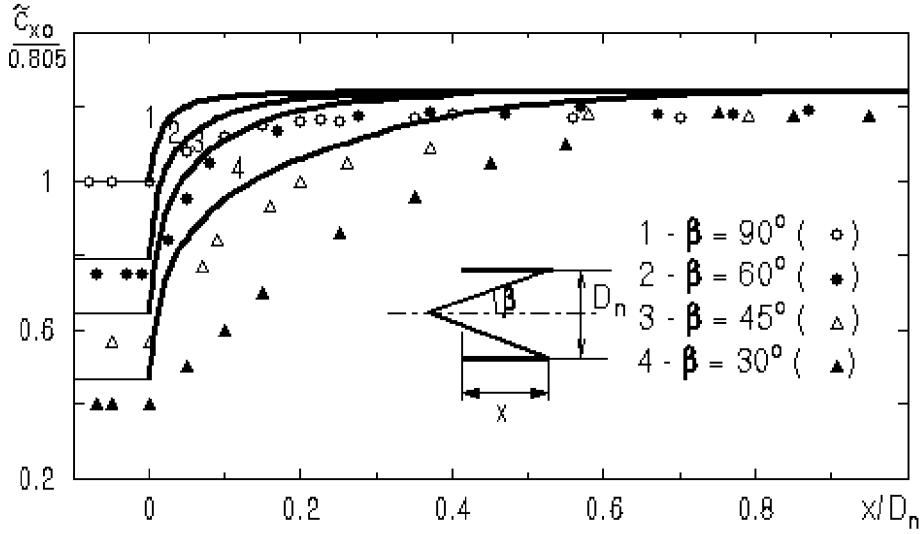
$\frac{\tilde{C}_{x0}}{0.805}$
1
0.6
0.2
0
0.2
0.4
0.6
0.8
x/D_n
1 - β = 90° (○)
2 - β = 60° (✱)
3 - β = 45° (△)
4 - β = 30° (▲)
β
D_n
X

Fig. 8

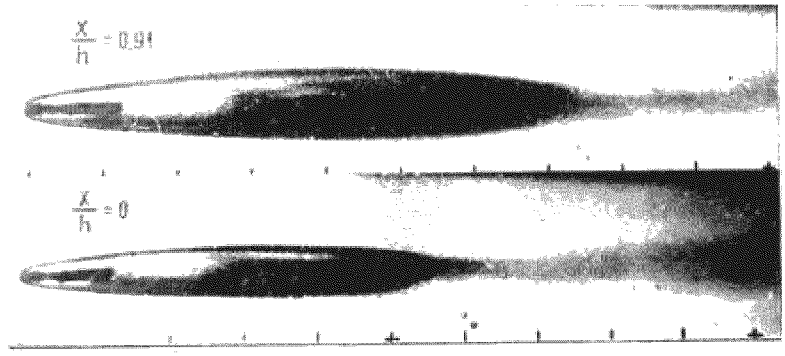
X/h = 0.91
X/h = 0

Fig. 9

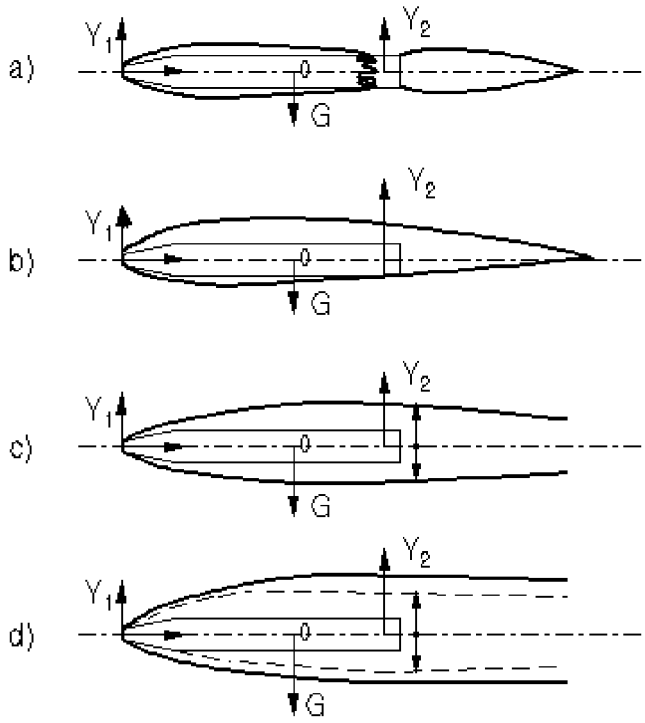

Fig. 10

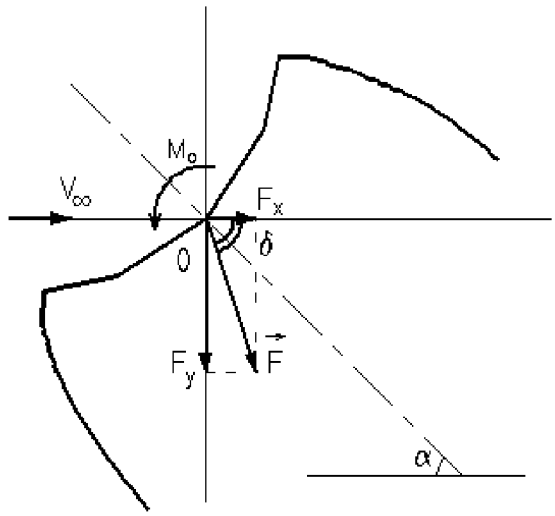

Fig. 11

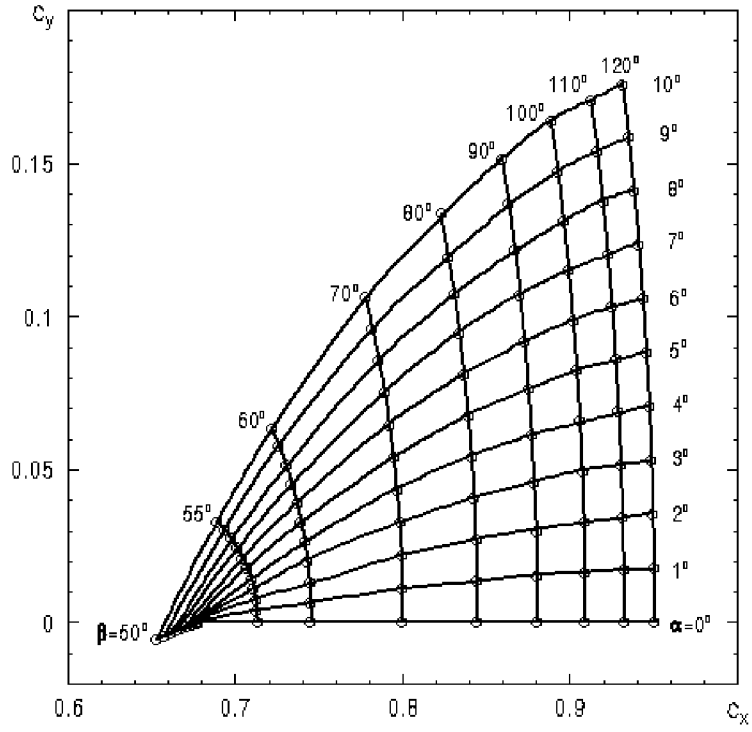
c_y
0.15
0.1
0.05
0
0.6
0.7
0.8
0.9
c_x
120°
110°
100°
90°
80°
70°
60°
55°
β=60°
10°
9°
8°
7°
6°
5°
4°
3°
2°
1°
α=0°

Fig. 12

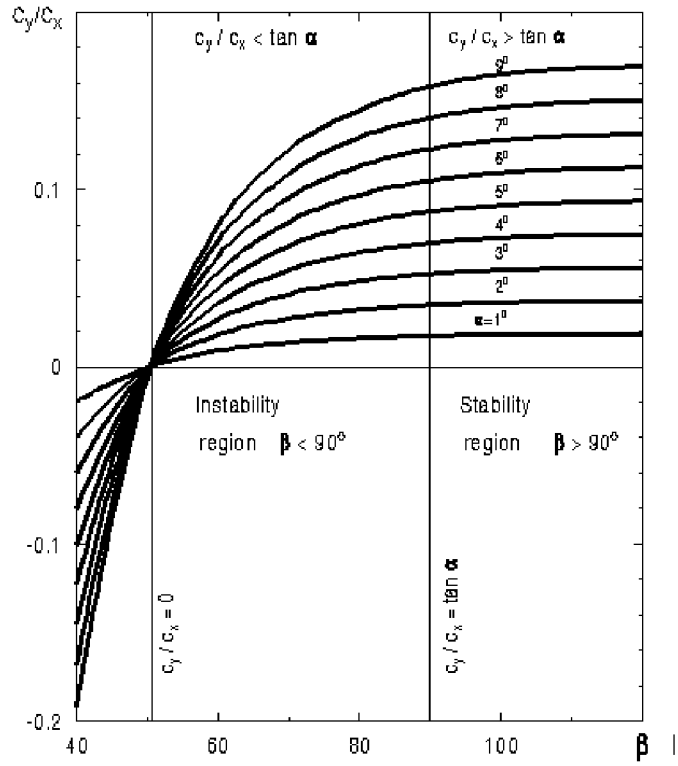
c_y/c_x
$c_y / c_x < \tan \alpha$
$c_y / c_x > \tan \alpha$
0.1
0
-0.1
-0.2
40
60
80
100
β
9°
8°
7°
6°
5°
4°
3°
2°
α=1°
Instability
region β < 90°
Stability
region β > 90°
$c_y / c_x = 0$
$c_y / c_x = \tan \alpha$

Fig. 13

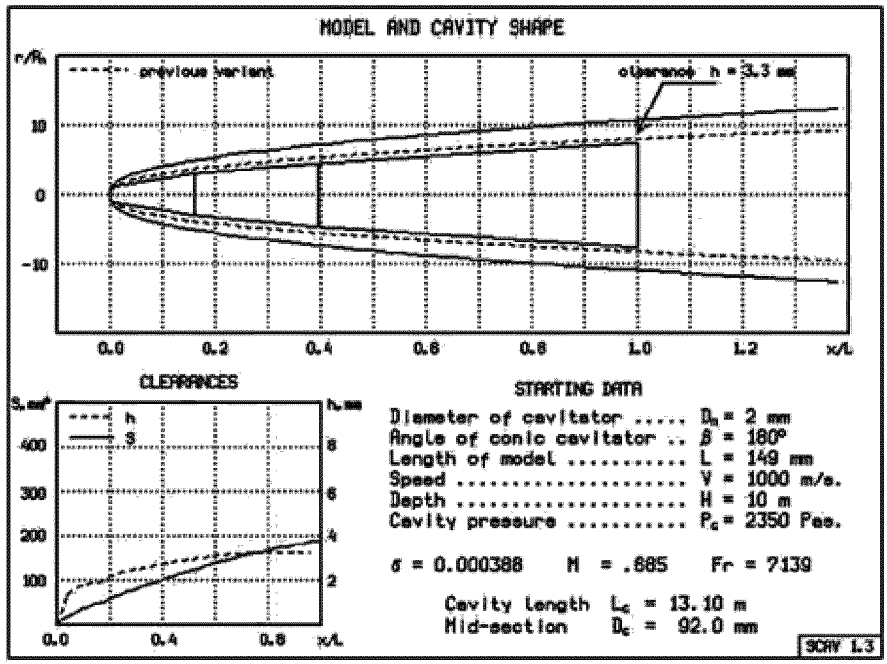
MODEL AND CAVITY SHAPE
r/R
previous variant
clearance h = 3.3 mm
10
0
-10
0.0
0.2
0.4
0.6
0.8
1.0
1.2
x/L
CLEARANCES
S, mm²
h, mm
h
S
400
300
200
100
8
6
4
2
0.0
0.4
0.8
x/L
STARTING DATA
Diameter of cavitator ..... D = 2 mm
Angle of conic cavitator .. β = 180°
Length of model ..... L = 149 mm
Speed ..... V = 1000 m/s.
Depth ..... H = 10 m
Cavity pressure ..... P = 2350 Pas.
σ = 0.000388 M = .885 Fr = 7139
Cavity length L = 13.10 m
Mid-section D = 92.0 mm
SCAV 1.3

Fig. 14

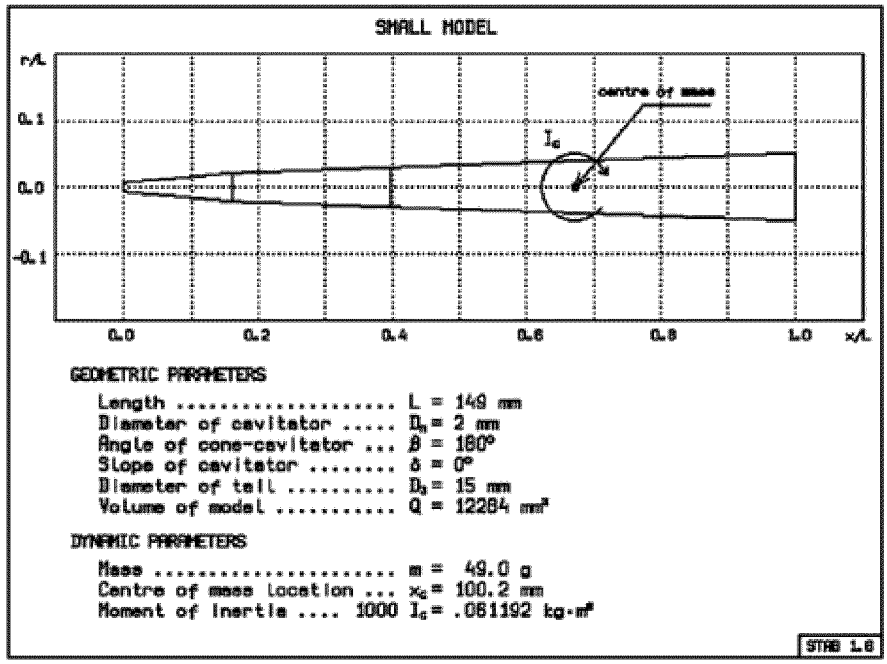
SMALL MODEL
r/L
centre of mass
0.1
0.0
-0.1
0.0
0.2
0.4
0.6
0.8
1.0
x/L
GEOMETRIC PARAMETERS
Length ..... L = 149 mm
Diameter of cavitator ..... D = 2 mm
Angle of cone-cavitator ... β = 180°
Slope of cavitator ..... δ = 0°
Diameter of tail ..... D = 15 mm
Volume of model ..... Q = 12284 mm³
DYNAMIC PARAMETERS
Mass ..... m = 49.0 g
Centre of mass location ... x = 100.2 mm
Moment of inertia .... 1000 I = .081192 kg·m²
STAB 1.8

Fig. 15

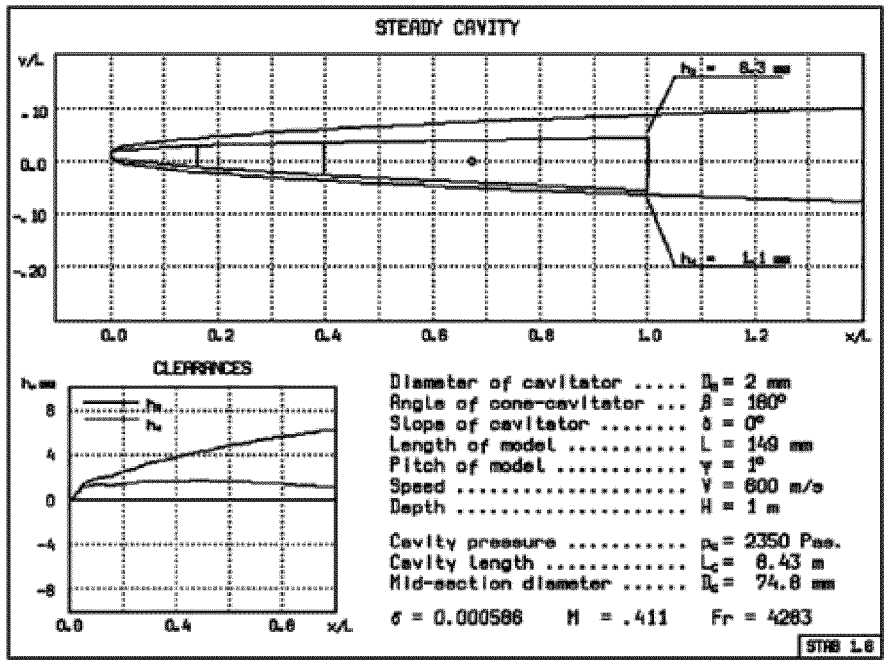
STEADY CAVITY
v/L
.10
0.0
-.10
-.20
0.0
0.2
0.4
0.6
0.8
1.0
1.2
x/L
CLEARANCES
h, mm
8
4
0
-4
-8
0.0
0.4
0.8
x/L
Diameter of cavitator ..... D = 2 mm
Angle of cone-cavitator ... β = 180°
Slope of cavitator ..... δ = 0°
Length of model ..... L = 149 mm
Pitch of model ..... ψ = 1°
Speed ..... V = 600 m/s
Depth ..... H = 1 m
Cavity pressure ..... p = 2350 Pas.
Cavity length ..... L = 8.43 m
Mid-section diameter ..... D = 74.8 mm
σ = 0.000586 M = .411 Fr = 4283
STAB 1.6

Fig. 16

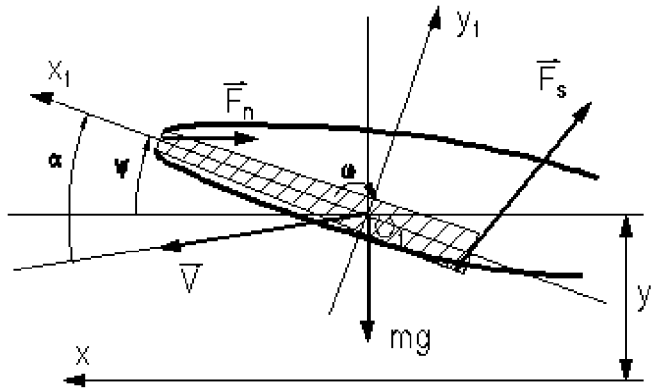
y1
x1
Fn
Fs
α
ψ
ω
V
y
mg
x

Fig. 17

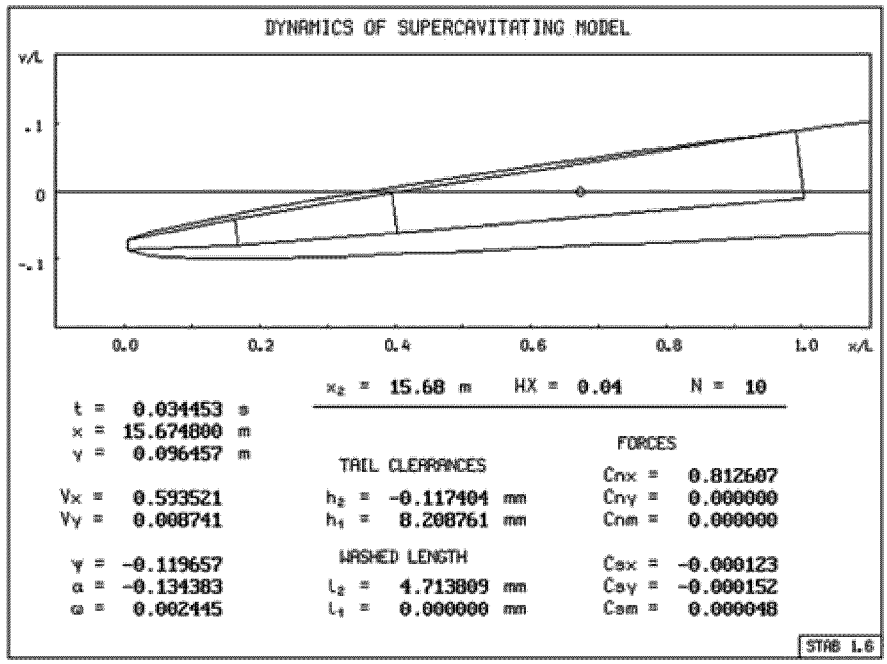

Fig. 18a

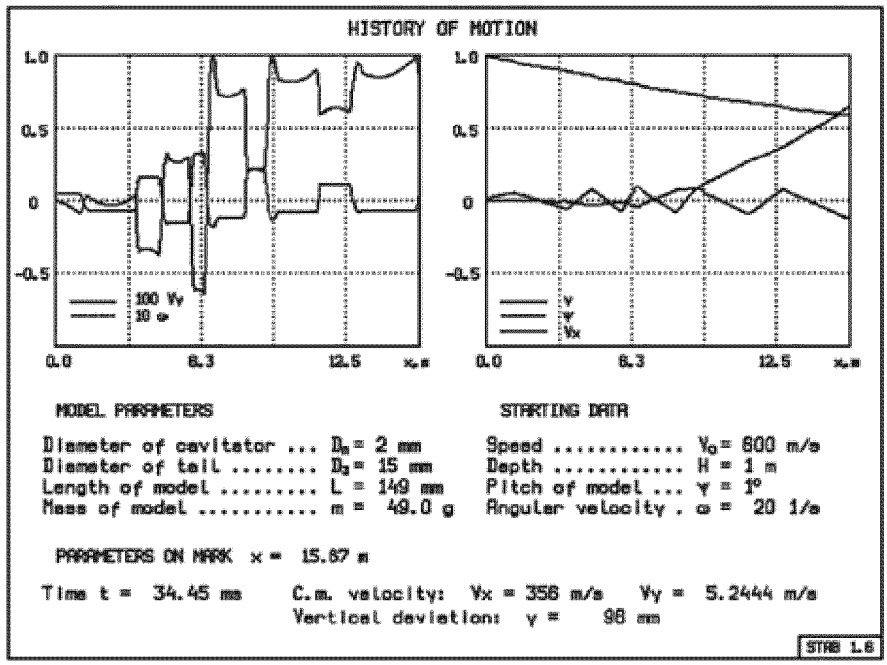

Fig. 18b

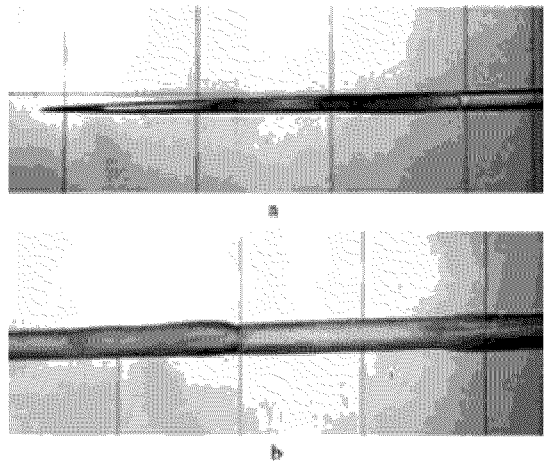

Fig. 19

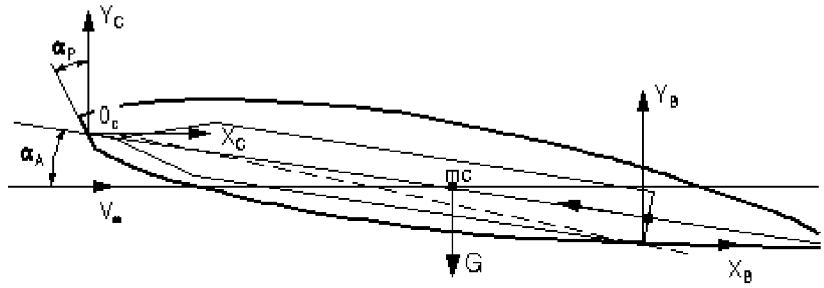

Fig. 20

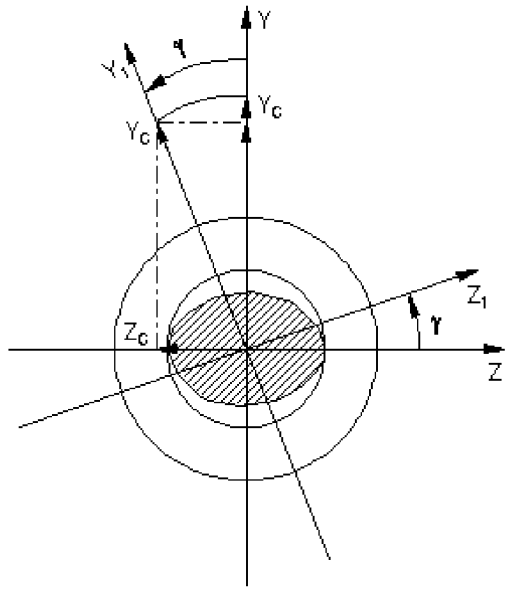

Fig. 21

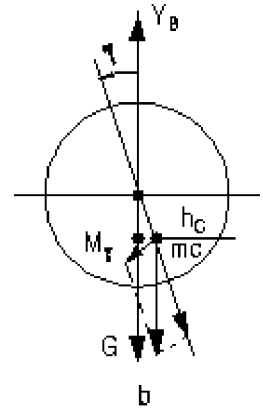

Fig. 22

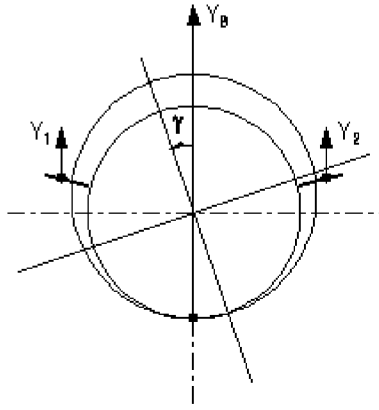

Fig. 23

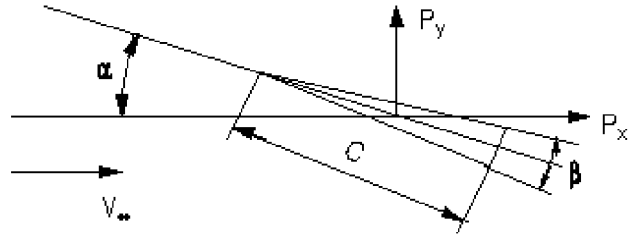

$$A = \frac{S}{C^2}$$

Fig. 24

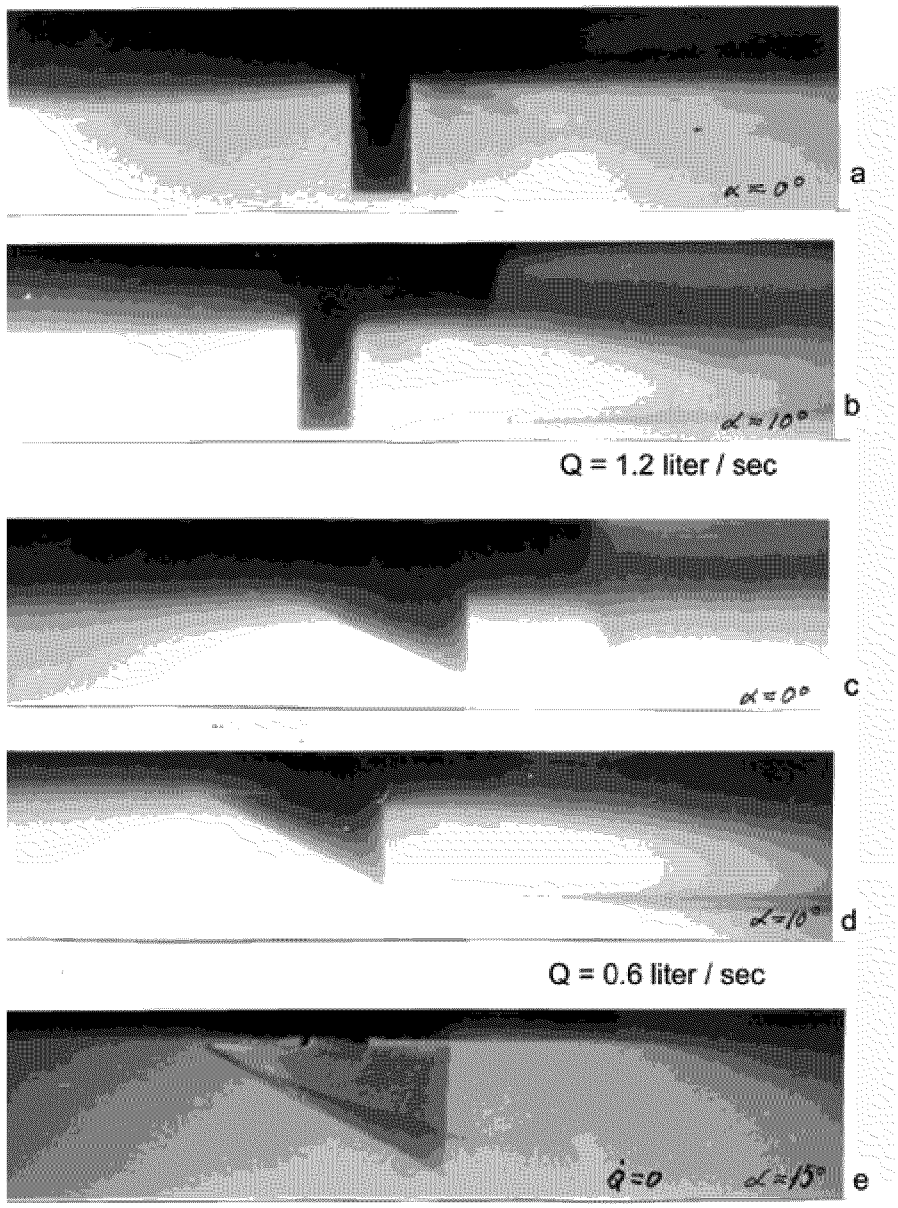

Fig. 25